On the mechanics of buckling–delamination in compliant laminates

R. H. J. Peerlings[1], E. D. Kleijne[1], E. van Veenendaal[2], P. C. P. Bouten[3]
[1]*Eindhoven University of Technology, Eindhoven, The Netherlands;*
[2]*Polymer Vision, Eindhoven, The Netherlands;*
[3]*Philips Research, Eindhoven, The Netherlands*

1 Introduction

Future generations of mobile electronic devices will contain flexible, bendable or even rollable displays. An example of such a device, which is already entering the market, is the Readius by Polymer Vision – see Figure 1(a). Apart from providing a range of exciting new options for designers, the introduction of ultra-flexible displays also presents a number of mechanical challenges to engineers, as the devices' reliability must be guaranteed despite the additional mechanical loading due to repeated bending and unbending.

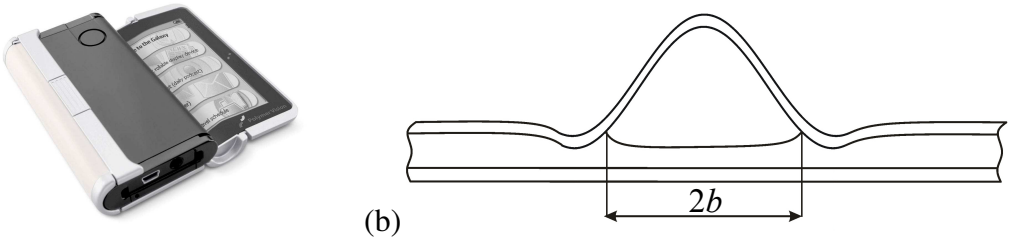

Figure 1: (a) Readius by Polymer Vision, containing a rollable display; (b) sketch of buckling–delamination in the stack of layers forming the display, where $2b$ is the width of the buckle and delamination zone.

In mechanical terms, the displays produced by Polymer Vision essentially consist of two polymer substrates which sandwich an extremely compliant active layer. The substrates each have a thickness of approximately 25 μm and an elasticity modulus on the order of a few GPa. The active layer is approximately 50 μm thick; its mechanical properties are not very well known, but its elastic modulus is certainly several orders of magnitude lower than that of the substrates.

Upon rolling, the inner substrate experiences a compressive stress. In one of the failure modes observed during prolonged and intensive testing, the substrate in compression buckles and simultaneously loses its adhesion to the soft intermediate layer (Figure 1(b)). This so-called buckling-driven delamination obviously compromises the integrity and functionality of the device.

The mechanics of buckling-driven delamination are well understood for films on stiff or thick substrates – see for instance the review by Hutchinson and Suo [1]. However, studies of films on compliant substrates have shown that the energy available for buckle formation in them may be significantly larger than predicted by the conventional theory [2–5].

Our objective is to predict the onset of buckling–delamination, as well as the propagation of the ensuing buckles, for thin laminates such as the rollable display of Figure 1. In particular, we are interested in predicting the influence of the relative stiffness and thickness of the compliant intermediate layer as compared to the top and bottom substrates.

Our analysis essentially follows that of Yu and Hutchinson [3]. Contrary to the semi-infinite substrates considered by these authors, however, we focus on thin substrates – of the same order of magnitude as the film – which are furthermore laminated. In the analysis, some simplifications are made with respect to that of Ref. [3], which we demonstrate to be justified by comparing predictions with full finite element simulations. Details of the analysis and further results are reported in a forthcoming publication [6].

2 Analysis

The problem which we consider is that of a straight buckle which is formed in the top layer of a three-layer planar laminate – see Figure 2(a). A compressive stress is introduced in the top layer by imposing a uniaxial thermal expansion in the direction of the x-coordinate. The resulting internal stress is characterised by the compressive mechanical strain away from the buckle, ε. Note that the thermal load is employed solely to introduce a state of stress which mimics that due to rolling of the display. The entire stack of materials is assumed to deform in a plane-strain mode. The top and bottom layer have the same thickness, h, and elastic properties, characterised by the plane-strain modulus $\bar{E}$. The intermediate layer has thickness h' and a plane-strain modulus $\bar{E}'$. We characterise the stiffness contrast by Dundurs's elastic mismatch parameter

$$\alpha = \frac{\bar{E} - \bar{E}'}{\bar{E} + \bar{E}'} \tag{1}$$

and are interested mostly in the case where $0 < \alpha < 1$, i.e. $\bar{E}' < \bar{E}$.

Following Yu and Hutchinson [3], we regard the delaminated and buckled part of the top layer, of width $2b$, as a plate in bending (Figure 2(b)). For the systems considered by us, however, it turns out that it is a reasonable assumption to decouple the compressive response and bending response of the plate. Instead of the von Kármán plate theory employed in [3], this allows us to use the standard Euler

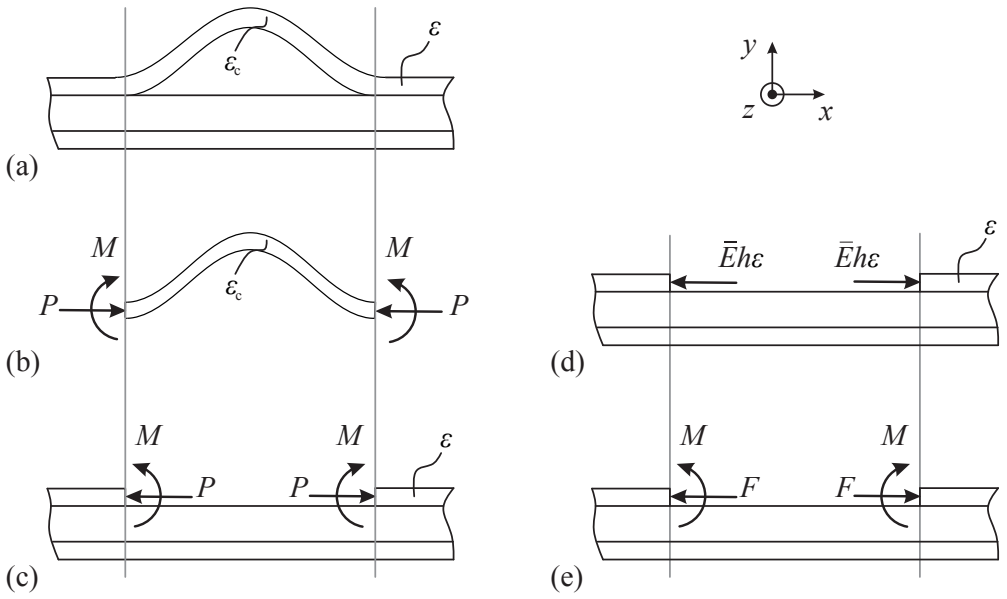

Figure 2: Decomposition of the buckling problem into subproblems: (a) full problem; (b) buckling of a compressed plate; (c) support of the plate, which can be further subdivided into (d) a uniform solution and (e) a correction to the uniform problem.

theory for buckling. The compressive strain in the buckle is constant and is assumed to remain equal to the strain at the onset of buckling, the critical buckle strain ε_c.

The main challenge of the analysis lies in characterising the boundary conditions of the plate used for the buckling analysis. Classically, a double-clamped condition is employed. However, the compliant intermediate layer in our system allows a significant amount of translation and rotation at the ends of the buckle. This compliance is governed by the remaining part of the three-layer system as sketched in Figure 2(c). The deformation and stress state in this remaining part can be subdivided into a uniform solution which corresponds to the unbuckled, but internally stressed state (Figure 2(d)) and a part which captures the additional deformation and stress due to the translation and rotation of the buckled layer (Figure 2(e)). The first subproblem requires a force per unit length $\bar{E}h\varepsilon$ at the interface with the buckle, so that for the second we have a force $F = P - \bar{E}h\varepsilon$ and moment M, where P and M are the force and moment acting on the buckle (Figure 2(b)).

Again following Yu and Hutchinson [3], the response of the remaining system as sketched in Figure 2(e) is characterised by

$$u = a_{11}\frac{F}{\bar{E}} + a_{12}\frac{M}{\bar{E}h} \tag{2}$$

$$\varphi = a_{21}\frac{F}{\bar{E}h} + a_{22}\frac{M}{\bar{E}h^2} \tag{3}$$

where u and φ are the displacement and rotation of the interface with the buckle respectively. The constants a_{11}, $a_{12} = a_{21}$ and a_{22} have been computed for a range of relative buckle widths b/h, intermediate layer thicknesses h'/h and stiffness contrasts α using the finite element model as sketched in Figure 3. In this model, the buckle has been replaced by a rigid body, to which a reference force F and moment M are successively applied in order to compute the coefficients a_{ij}. A similar model which also includes the buckle has been used to numerically generate reference solutions.

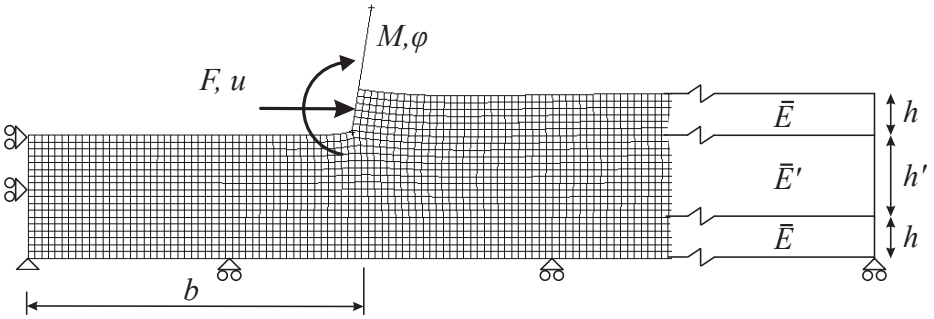

Figure 3: Finite element model used to compute the boundary compliance coefficients a_{ij} featuring in Equations (2)–(3).

Figure 4 shows the values computed for a_{11} and a_{22} using the finite element model as a function of b/h and for stiffness contrasts α ranging from 0.5 to 0.99. The ratio b/h has been varied by changing the (semi-)buckle width b at constant h and α by changing $\bar{E}'$ at constant $\bar{E}$. The data reported in the figure is for a intermediate layer thickness of $h' = 2h$, which is realistic (see Section 1). The computed a_{12} (not shown here) turn out to be substantially smaller than a_{11} and a_{22}, allowing us to neglect the coupling terms in (2)–(3).

As in the results obtained by Yu and Hutchinson [3] for a semi-infinite substrate, the coefficient a_{22} does not vary appreciably with b/h (Figure 4(b)). The influence of the stiffness contrast α is intuitive: a more compliant intermediate layer (i.e. a higher α) results in more rotation of the buckle ends (higher a_{22}).

The influence of α on the translational compliance a_{11} is similar to that on a_{22} (Figure 4(a)). However, here we observe a clear influence of the buckle width b, which appears to be virtually linear. This can be understood by realising that upon formation of the buckle, the relatively thin intermediate and bottom layers below it can largely relax along the entire width of the buckle. These two layers thus act as a spring, the compliance of which scales linearly with b. Note that this effect is absent for the semi-infinite substrate considered by Yu and Hutchinson [3], in which the response must become uniform for $y \to -\infty$.

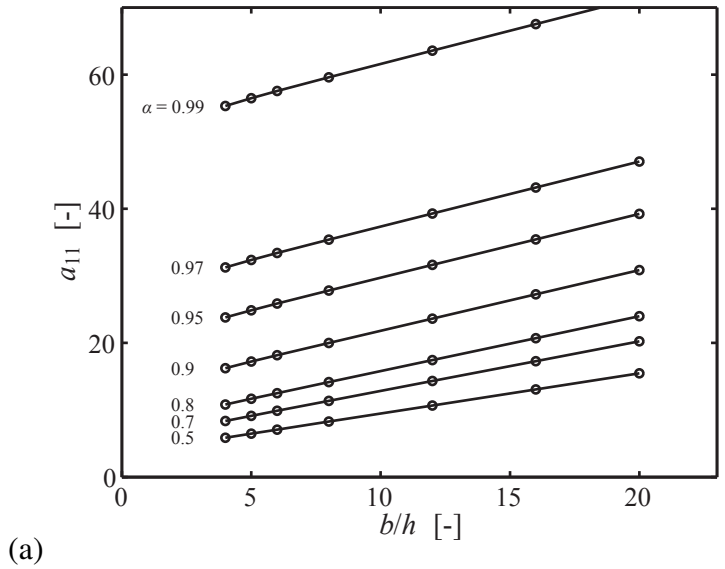

(a)

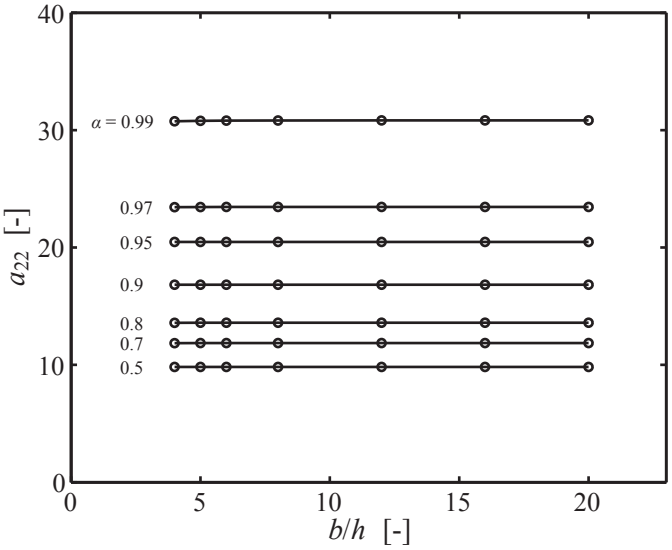

(b)

Figure 4: Computed boundary compliance coefficients (a) a_{11} and (b) a_{22} as a function of the normalised buckle width b/h for $h' = 2h$ and various values of the stiffness contrast α.

An interesting observation can be made by correcting the translational compliance a_{11} for the relaxation mechanism as discussed above. To this end, define a local translational compliance coefficient $\tilde{a}_{11}$ as follows:

$$\tilde{a}_{11} = a_{11} - \left(1 + \frac{1-\alpha}{1+\alpha}\frac{h'}{h}\right)^{-1} \frac{b}{h} \tag{4}$$

The second term in this expression represents the compliance associated with the intermediate and bottom layers below the buckle; it can be derived in a straightfor-

ward fashion from the elastic stiffness of the two layers in parallel and expressing it in terms of the stiffness contrast α. Applying this relation to the data of Figure 4(a) results in the diagram of Figure 5(a). It shows that, like a_{22}, the coefficient $\tilde{a}_{11}$ is independent of b/h.

The remaining constants characterising the buckle's boundary conditions, $\tilde{a}_{11}$ and a_{22}, have been plotted on a double-logarithmic scale in Figure 5(b). Apart from the

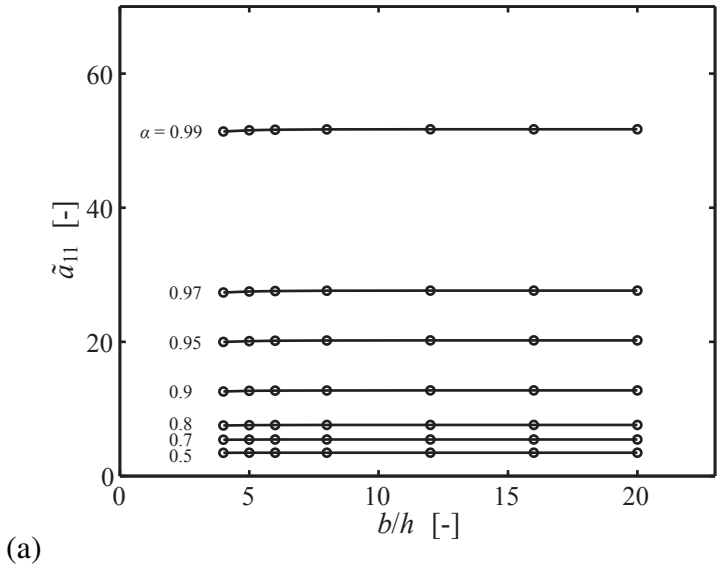

(a)

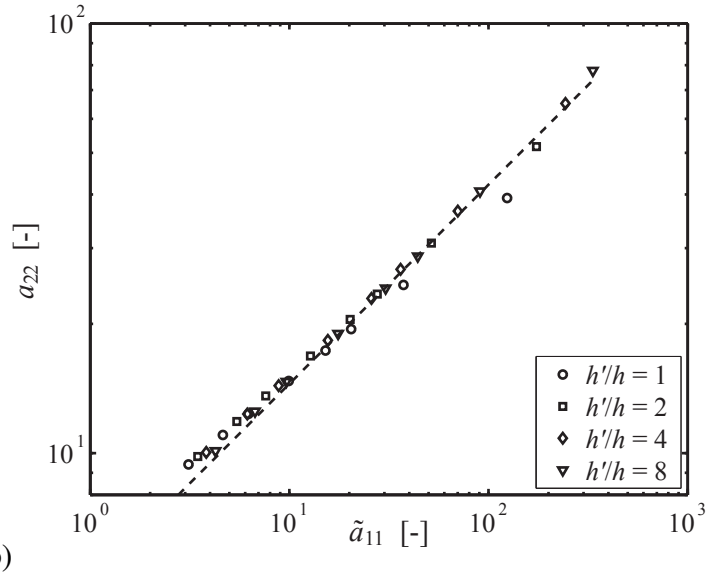

(b)

Figure 5: (a) Local translational compliance coefficient $\tilde{a}_{11}$ obtained from relation (4). (b) Rotational compliance a_{22} vs local translational compliance $\tilde{a}_{11}$ for a range of relative layer thicknesses and stiffness contrasts; the dashed line indicates a possible square-root dependence.

data of Figures 4(b) and 5(a), also values obtained for other thickness ratios h'/h are included in the diagram. The data clearly suggests a direct relationship between the two coefficients, which appears to be described quite closely by $a_{22} \propto \sqrt{\tilde{a}_{11}}$, as evidenced by the dashed line of slope $1/2$ in the diagram. Efforts to further clarify this relation and to make a connection with the properties of the respective layers of the laminate are in progress.

Now that the compliance coefficients a_{11} and a_{22} have been determined, we can turn our attention to predicting the onset of buckling and the ensuing buckle shape. For this purpose consider the buckled part of the top layer as sketched in Figure 2(a). Its deflection $w(x)$ must satisfy the differential equation

$$\tfrac{1}{12}\bar{E}h^3\frac{\mathrm{d}^2 w}{\mathrm{d}x^2} + Pw = M \tag{5}$$

Solving this equation for $w(x)$, using the symmetry condition $\mathrm{d}w/\mathrm{d}x|_{x=0} = 0$ and $w(b) = 0$, results in

$$w = \hat{w}\left(1 - \frac{\cos\frac{\pi x}{\lambda}}{\cos\frac{\pi b}{\lambda}}\right) \tag{6}$$

where

$$\hat{w} = w(0) = \frac{M}{P} \qquad \text{and} \qquad \lambda = \tfrac{1}{2}\pi h\sqrt{\frac{\bar{E}h}{3P}} \tag{7}$$

The unknown λ may be obtained by setting the rotation at $x = b$ as given by the derivative of (6) equal to the angle φ according to (3). After some algebra this results in the following equation for λ:

$$\frac{\lambda}{b}\tan\frac{\pi b}{\lambda} = -\tfrac{1}{12}\pi a_{22}\frac{h}{b} \tag{8}$$

This equation cannot be solved in closed form, but a reasonably accurate approximation can be obtained by a first-order Taylor expansion of $\tan \pi b/\lambda$ around $\lambda/b = 1$; this results in

$$\lambda = \tfrac{1}{2}b\left(1 + \sqrt{1 + \tfrac{1}{3}a_{22}\frac{h}{b}}\right) \tag{9}$$

The critical buckling strain ε_c follows from the assumption that $P = \bar{E}h\varepsilon_\mathrm{c}$ as

$$\varepsilon_\mathrm{c} = \tfrac{1}{12}\pi^2\frac{h^2}{\lambda^2} \tag{10}$$

Note that for a rigid substrate, for which $a_{22} = 0$ and thus $\lambda = b$, we recover the classical result which for further reference we denote ε_*. Since for compliant supports ($a_{22} > 0$) we have $\lambda > b$, expression (10) predicts buckling to occur

earlier (at a smaller applied strain) than the buckling strain ε_* obtained for a rigid substrate – as would be expected for compliant boundary conditions.

The buckle height $\hat{w}$ is obtained via the usual arguments and reads

$$\hat{w} = \frac{4}{\pi} b \sqrt{\left(1 + a_{11}\frac{h}{b}\right)(\varepsilon - \varepsilon_c)} \tag{11}$$

Note that the compliance of the buckle's supports enters this expression via a_{11} as well as via the critical buckle strain ε_c, which via (9) and (10) depends on a_{22}. Setting $a_{11} = a_{22} = 0$ again results in the classical expression for a rigidly supported buckle. Compared with it, relation (11) predicts a higher buckle at the same applied strain ε.

Now that the buckled solution is available, we can also determine the energy release rate associated with steady-state propagation of the buckle, G_{ss}. It is this value, relative to the toughness of the interface between the top and intermediate layers, which determines whether a straight buckle will grow longitudinally – see e.g. [1]. For the system considered here it can be estimated as [6]

$$G_{ss} = \tfrac{1}{2}\bar{E}h\left(1 + a_{11}\frac{h}{b}\right)(\varepsilon - \varepsilon_c)^2 \tag{12}$$

Note again the influence of compliance in this expression; for $a_{11} = a_{22} = 0$ the result for a rigid substrate is retrieved – e.g. [1].

3 Preliminary results

Preliminary results of the semi-analytical model as discussed above are presented in Figure 6. It shows the buckle height $\hat{w}$ (Figure 6(a)) and the steady-state energy release rate G_{ss} (Figure 6(b)) as a function of the applied strain ε and for a range of stiffness contrasts α. A relative buckle width of $b/h = 16$ and intermediate layer thickness of $h'/h = 2$ have been used; see Reference [6] for a study on the influence of these parameters and further results. Predictions made by the semi-analytical model, given as solid curves, are compared with data obtained from finite element simulations of the full buckling problem (dotted curves). The well-known analytical results for a rigid substrate (or $\alpha = -1$) are indicated as dashed curves. The axes of both diagrams have been made dimensionless using the classical critical buckling strain (for rigid substrates) ε_*, the top layer thickness h and the reference energy $G_0 = \frac{1}{2}\bar{E}h\varepsilon^2$; the latter represents the maximum amount of energy which can be released from solely the top layer over a width $2b$.

Figure 6(a) shows that for compliant intermediate layers buckling indeed occurs at strain levels which are lower than the classical limit $\varepsilon/\varepsilon_* = 1$. This trend is slightly underestimated by the semi-analytical model compared to the finite element

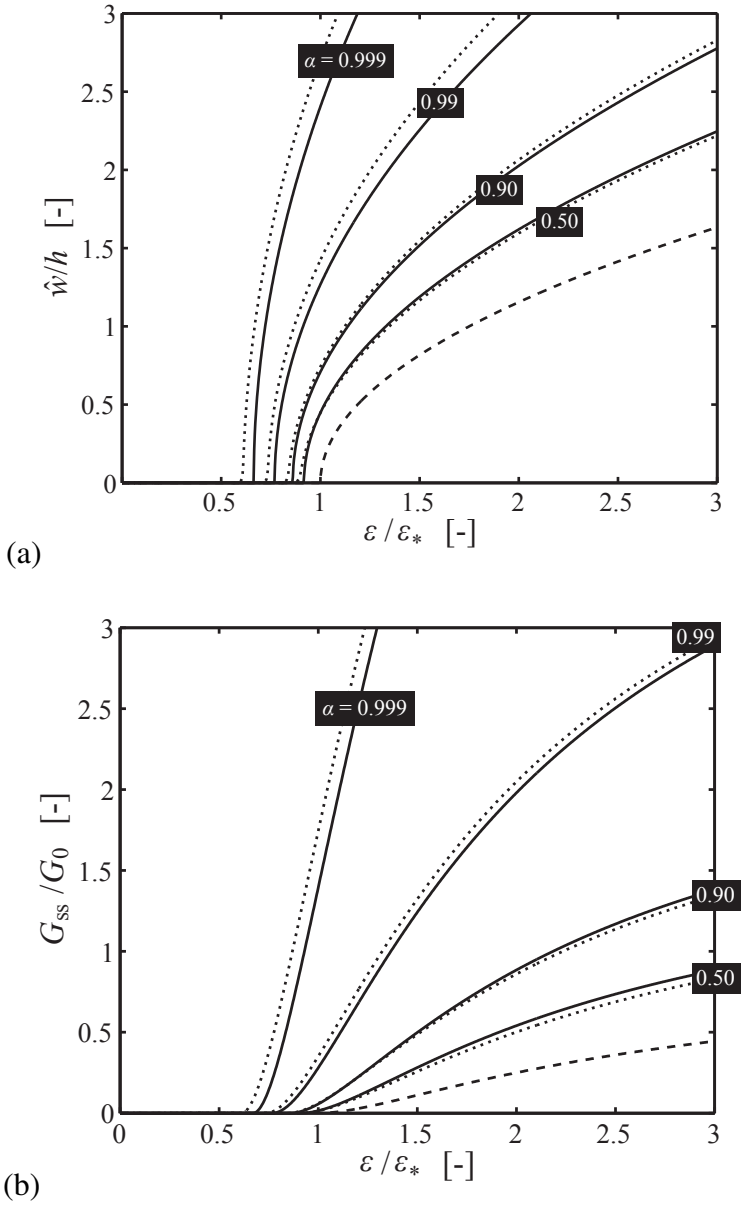

Figure 6: Results obtained with the semi-analytical model (solid curves) as compared to full finite element simulations (dotted curves): (a) normalised buckle height and (b) normalised steady-state energy release rate vs normalised applied strain for $b = 16h$, $h' = 2h$ and various levels of stiffness contrast. The dashed curves represent the classical solution for a rigid substrate ($\alpha = -1$).

simulations. The increase of the buckle height as the applied strain is increased is captured rather well by the semi-analytical model. The buckle heights reached are dramatically higher for compliant intermediate layers than for the rigid support implied by the analytical solution (dashed curve).

A similar effect is observed for the energy release rate G_{ss} in Figure 6(b). The energy released upon buckle propagation is substantially higher for systems with a more compliant intermediate layer. Note that the fact that $G_{ss}/G_0 > 1$ for such systems indicates that a significant amount of energy is released from the bottom layer, as well as from the top layer beyond the buckle width $2b$. The freedom introduced by a compliant intermediate layer allows a larger region around the buckle to relax and thus release energy. This trend is picked up well by the semi-analytical model, as evidenced by the small difference with the finite element results.

4 Concluding remarks

The results of the previous section demonstrate that predictions made by the conventional buckling–delamination theory are grossly inaccurate for laminates which contain compliant layers. Compared with the semi-infinite compliant substrate considered by Yu and Hutchinson [3], additional mechanisms come into play for the thin structure considered here. In particular, the layers below the buckle can relax more freely than in the semi-infinite case and thus contribute more to the driving force for buckle propagation, the steady-state energy release rate.

Apart from the energy release rate for steady-state propagation, the release rate associated with an increase of the buckle width can also be extracted from the present analysis. This allows one to study the competition between buckle growth in longitudinal and lateral direction, and thus to determine the natural width of buckles in a given system – see the discussion by Yu and Hutchinson [3] and, for results for thin laminates, Kleijne et al. [6].

References

[1] J. W. Hutchinson, Z. Suo, Mixed mode cracking in layered materials, Advances in Applied Mechanics 29(1992) 63–191

[2] B. Cotterel, Z. Chen, Buckling and cracking of thin films on compliant substrates under compression, International Journal of Fracture 104(2002) 169–179

[3] H.-H. Yu, J. W. Hutchinson, Influence of substrate compliance on buckling delamination of thin films, International Journal of Fracture 113(2002) 39–55

[4] G. Parry, J. Colin, C. Coupeau, F. Foucher, A. Cimetière, J. Grilhé, Effect of substrate compliance on the global unilateral post-buckling of coatings: afm observations and finite element calculations, Acta Materialia 53(2005) 441–447

[5] P. C. P. Bouten, M. A. J. van Gils, Buckling failure of compressive loaded hard layers in flexible devices, in: Materials Research Society Symposium Proceedings, vol. 843, pp. 105–110

[6] E. D. Kleijne, R. H. J. Peerlings, P. C. P. Bouten, E. van Veenendaal, Buckling mechanics of thin films on thin compliant substrates (2008). In preparation